

Removal of phosphate from water using lanthanum-modified coal gangue

Jianmin Zhou^a, Yongsheng Fu^a, Mengyao Zhang^a, Yiqing Liu^{a,*}, Shuhang Ding^a, Li Zhao^b

^aSchool of Geoscience and Environmental Engineering, Southwest Jiaotong University, Chengdu, Sichuan 611756, China, Tel. +86-18081171718; email: swjtu7001@163.com (Y. Liu), Tel. +86-13408460797; email: 245960737@qq.com (J. Zhou), Tel. +86-13908038700; email: fuys@home.swjtu.edu.cn (Y. Fu), Tel. +86-13258327739; email: 614725344@qq.com (M. Zhang), Tel. +86-13076097361; email: 447452334@qq.com (S. Ding)

^bCollege of Water Conservancy and Hydropower Engineering, Sichuan Agricultural University, Ya'an 625014, China, Tel. +86-15983608666; email: fangling4081@163.com (L. Zhao)

Received 26 April 2020; Accepted 9 September 2020

ABSTRACT

Lanthanum-modified coal gangue (LMGC) prepared by a hydrothermal method was used to remove phosphate from water. The structure and properties of LMGC were characterized by X-ray diffraction (XRD), attenuated total reflection Fourier transform infrared spectroscopy (ATR-FTIR), and transmission electron microscopy. The pH value greatly affects the phosphate removal ability of LMGC. When the pH value is 3–7, the phosphate removal efficiency is more than 75%; when the pH value is 5, the phosphate removal efficiency is maximal (84.40%). Langmuir and Freundlich models were used to describe the isotherm, and the isotherm constant was determined. The results show that Langmuir isotherm well described the isotherm adsorption of phosphate, and the maximum adsorption capacity was 78.66, 80.58, and 83.83 mg/g at 20°C, 30°C, and 40°C, respectively. The thermodynamics study shows that the adsorption process is a spontaneous endothermic reaction. According to the XRD, X-ray photoelectron spectroscopy (XPS), and ATR-FTIR results, the adsorption mechanism of phosphate was mainly the formation of complexes via ligand exchange. This study suggests that LMGC is a novel phosphorus-removing agent with low cost, high adsorption capacity, and high selectivity. Its application can reduce the discharge of coal gangue and promote its high added value utilization for water pollution treatment.

Keywords: Coal gangue; Lanthanum; Phosphate; Adsorption kinetics; Adsorption isotherm; Mechanism

1. Introduction

As we know, the excessive discharge of sewage and agricultural nonpoint source pollution causes the eutrophication problem of the receiving water body, where nitrogen and phosphorus are the key elements [1]. In the eutrophication process, nitrogen is reduced to nitrous oxide through denitrification and leaves the water body, while phosphorus is difficult to remove from water. In addition, cyanobacteria and green algae will reproduce in large quantities and fix nitrogen from the air in the presence of excess phosphorus [2]. Therefore, the concentration of phosphorus becomes

an important pollution index in the development stage of lake eutrophication [3], and it is very important to control the phosphorus emission to reduce eutrophication.

Currently, there are many methods to remove phosphorus from water, including physicochemical methods (e.g., coagulation [4–6] and adsorption [7,8]), biological methods (e.g., A/O, A²/O, BAF [9], MBR [10], and other biologically strengthening methods [11]), ecological treatment methods such as artificial wetland [12], the ecological floating island [13] and aquatic plant restoration [14], and the combination of these methods [15,16]. Among these methods, adsorption has attracted increasing attention because of its

* Corresponding author.

high efficiency, simple operation, low secondary pollution, and recyclability. The adsorbent is the core of adsorption. Recently, many adsorbents such as porous metal oxide [17], porous metal hydroxide [18], MOFs [19], biologically activated carbon [20,21], clay mineral material [22–25], graphene [26], and relatively cheap industrial solid waste [27] were studied for the phosphorus removal. Porous metal oxides, MOFs, and graphene are always difficult to prepare, some industrial waste adsorption materials are insufficient in raw materials and purification, and there is a lack of mineral resources to prepare mineral adsorbents. Therefore, it is a hot spot to search for efficient, cheap, easy-to-obtain, sufficient raw materials, and economically feasible adsorbents.

Coal gangue is a type of solid waste in the mining and washing process of raw coal. Its main chemical composition is Al_2O_3 , SiO_2 , Fe_2O_3 , Na_2O , K_2O , CaO , MgO , and other oxides, and its main mineral components are kaolinite, montmorillonite, illite, chlorite, calcite, and boehmite. Kaolinite and montmorillonite are the main clay minerals of coal gangue. In China, the stock and emission of coal gangue are very large. By 2017, the cumulative stock of coal gangue was 7 billion tons [28], and its annual emission continues to increase with more than 300 million tons [29]. The long-term storage of coal gangue occupies large amounts of valuable land resources and damages the ecological environment of the mining area. In recent years, research on the utilization of coal gangue has developed, but there is less research on the environment. The research on environmental utilization mainly focuses on the preparation of coagulant and the removal of heavy metals and pigments, but there are few reports on the removal of phosphorus from water by coal gangue.

Because gangue is rich in clay minerals, lanthanum-modified coal gangue (LMCG) was successfully prepared and used to remove phosphorus from water. The composition, characteristic, and adsorption mechanism of this prepared material were analyzed by X-ray diffraction (XRD), X-ray fluorescence (XRF), X-ray photoelectron spectroscopy (XPS), transmission electron microscopy (TEM), and scanning electron microscopy (SEM). The effect of pH and coexisted ions on the adsorption performance of LMCG was also analyzed. Finally, the adsorption mechanism was explored by investigating the adsorption kinetics, thermodynamics, and adsorption isotherm.

2. Materials and methods

2.1. Materials

Coal gangue was taken from Sichuan GuXu Coal Field Development Co., Ltd. (China). The original coal gangue

was first manually separated to remove the impurities and white gangue; then, it was milled to 160 mesh by ball mill. The main components of coal gangue are shown in Table 1. The chemical reagents in the experiment were hydrochloric acid (HCl), potassium dihydrogen phosphate (KH_2PO_4), potassium antimony tartrate ($\text{K}(\text{SbO})\text{C}_4\text{H}_4\text{O}_6 \cdot 1/2\text{H}_2\text{O}$), potassium sodium tartrate ($\text{KNaC}_4\text{H}_4\text{O}_6 \cdot 4\text{H}_2\text{O}$), ammonium molybdate ($(\text{NH}_4)_6\text{Mo}_7\text{O}_{24} \cdot 4\text{H}_2\text{O}$), ascorbic acid ($\text{C}_6\text{H}_8\text{O}_6$), lanthanum nitrate ($\text{La}(\text{NO}_3)_3 \cdot 6\text{H}_2\text{O}$), and ammonia water, which were analytically pure and purchased from Chengdu Jinshan Chemical Reagent Company in Chengdu, China.

2.2. Material preparation

First, 20 g of 160 mesh coal gangue was placed into a corundum crucible and calcined at 800°C in a muffle furnace with a heating rate of $5^\circ\text{C}/\text{min}$ for 2 h. Then, it was removed and cooled to room temperature in air to obtain thermally activated coal gangue (TACG). Afterwards, 5 g of TACG was dispersed in 175 mL of 0.2 mol/L lanthanum nitrate solution, and it was stirred at 400 rpm in a water bath at 40°C for 5 min. Next, the mixed solution pH was adjusted to 10 using ammonia water, and stirring continued for 2 h in the water bath. Finally, the sediment was repeatedly washed in a centrifuge at 4,000 r/min and dried at 105°C for 12 h to obtain LMGC. Their main chemical compositions are shown in Table 1.

2.3. Material characterization

In this study, the phase changes of the adsorbent before and after adsorption were analyzed by a Smartlab 9-kw X-ray diffractometer (XRD, Rigaku, Japan). The SU8100 SEM (Hitachi) and JEM2100X TEM (JEOL) were used to analyze the morphology characteristics of the adsorbents. The chemical states and main elements of the surface of the adsorbent before and after adsorption were analyzed by an AXIS ULTRA DLD XPS spectrometer (Shimadzu). The chemical compositions of the materials were analyzed by an Epsilon 3XLE energy-dispersive X-ray fluorescence spectrometer (XFS, PANalytical, Netherlands). The functional groups and chemical bonds on the surface of the sample were determined using an I550 FTIR spectrometer (Thermofisher, United States).

2.4. Experiment on adsorption properties of phosphate

The adsorption experiments were performed in a 250 mL Erlenmeyer flask, where 100 mL phosphate solution and 1 g/L adsorbent were added at pH 7 in a thermostatic shaker bath of 180 rpm. The reaction temperature was 30°C

Table 1
Main chemical composition of coal gangue and its modified materials

Composition (%) materials	SiO_2	Al_2O_3	Fe_2O_3	CaO	TiO_2	MgO	Na_2O	K_2O	La_2O_3
Coal gangue	43.97	18.43	14.75	12.11	4.45	2.18	1.63	1.34	–
Thermally activated coal gangue	41.54	19.98	14.33	12	4.44	1.92	0.90	1.10	0.003
Lanthanum-modified coal gangue	14.67	6.29	8.02	2.20	2.20	0.28	0	0.46	63.34

unless otherwise specified. Then, 0.1 M HCl or 0.1 M NaOH solutions were added to adjust the initial pH to explore the effect of the initial solution pH at the initial phosphate concentration of 50 mg/L. CaCl₂, NaCl, MgCl₂, Na₂CO₃, Na₂SO₄, NaNO₃, and NaF were used as the source of coexisting anions to study the effect of coexisting ions. The concentration of coexisting ions was set up to 100 mg/L at the initial phosphate concentration of 50 mg/L. The experimental time of pH value and coexisting ions was 2 h. The kinetics test method of multi-bottle was used in this experiment with initial PO₄-P concentrations of 5, 25, and 50 mg/L, respectively. The sample was extracted from the solution to measure the concentration at predetermined time points (0.25, 0.5, 1, 2, 3, 5, 7, 9, 11, 13, 16, 20, and 24 h). In the isothermal adsorption experiment, the Erlenmeyer flask was shaken for 24 h to ensure adsorption equilibrium at 20°C, 30°C, and 40°C. The adsorption capacity of the adsorbent (q) and removal efficiency (R) of PO₄-P were calculated according to Eqs. (1) and (2), respectively.

$$q = \frac{C_0 - C_e}{m} \times V \quad (1)$$

$$R = \frac{C_0 - C_e}{C_0} \times 100 \quad (2)$$

where q is the adsorption capacity of the adsorbent, mg/g; R is the removal efficiency of PO₄-P (%); C_0 and C_e are the initial and residual concentrations of PO₄-P (mg/L); m is the mass of the adsorbent (g); V is the volume of the adsorbate (L).

3. Results and discussion

3.1. Characteristics of LMGC

The ATR-FTIR analysis of LMGC is shown in Fig. 1a. There were obvious absorption peaks near 3,608; 3,431; 2,925; 1,631; 1,469; 1,403; 853; and 634 cm⁻¹. The absorption peak of 3,608 cm⁻¹ was attributed to the hydroxyl stretching vibration of La-OH [30], which further confirms that lanthanum hydroxide was successfully loaded on the surface of coal gangue. The peaks near 3,431 and 1,631 cm⁻¹ belong to the stretching vibration and bending vibration of adsorbed water, respectively. The peak near 1,469 cm⁻¹ was attributed to the vibration of CO₃²⁻, which might be caused by the dissolution of CO₂ during the modification. The peak near 1,403 cm⁻¹ was formed by the vibration of NO₃⁻, which might be from the use of a modifier (lanthanum nitrate) in the modification process. The absorption peaks near 853 and 634 cm⁻¹ were ascribed to the vibration of the La-O bond in La₂O₃ [31] and La(OH)₃ [32], respectively, which suggests that although La(OH)₃ was loaded on the surface of coal gangue, lanthanum might enter the inner structure of coal gangue. However, the crystal phase of La₂O₃ was not found in the XRD spectrum of LMGC, which indicates that no lanthanum oxide was formed, and the La-O bond at 853 cm⁻¹ might be due to the combination of lanthanum with oxygen in the inner structure of coal gangue.

The XRD spectrum of LMGC is shown in Fig. 1b. The main phases of the modified material were lanthanum hydroxide (La(OH)₃) and quartz. 2θ = 15.719°, 27.880°, 31.460°, 47.058°, and 48.420° were the characteristic peaks of lanthanum hydroxide, which belong to the (100), (101), (200), (002), and

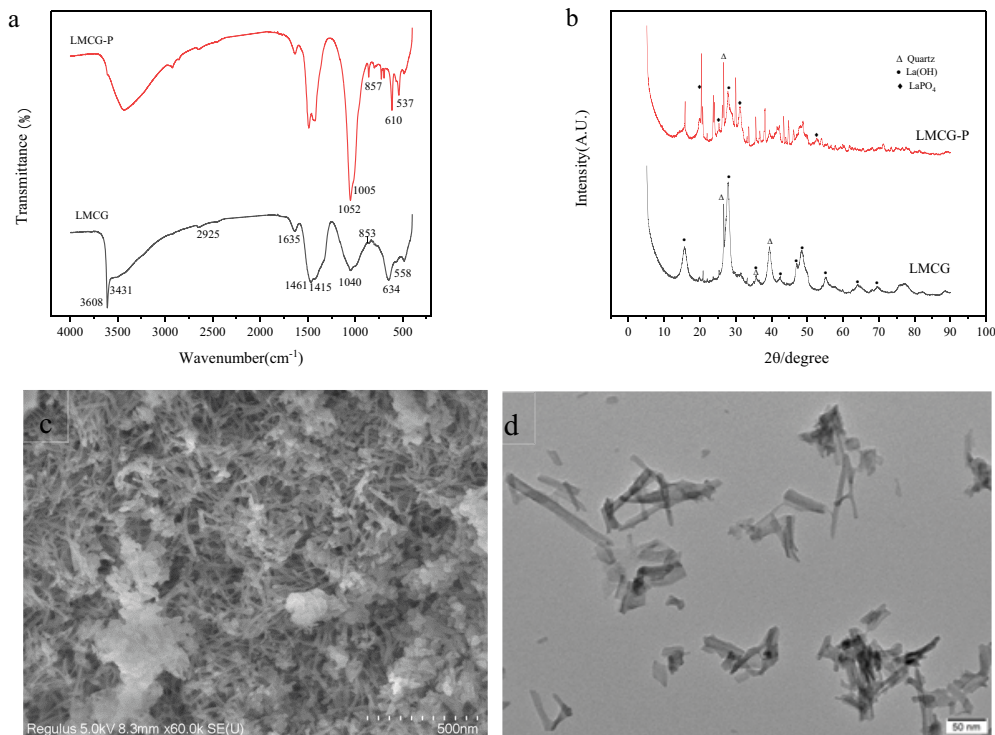


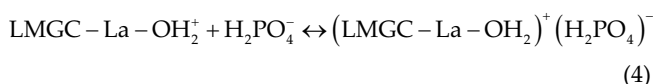
Fig. 1. ATR-FTIR spectras (a), XRD patterns (b) for LMGC before and after phosphate adsorption, SEM image (c) and TEM image (d) of LMGC (LMGC before phosphate adsorption, LMGC-P after phosphate adsorption).

(300) faces of the $\text{La}(\text{OH})_3$ crystal, respectively. The characteristic peaks of quartz were at $2\theta = 20.819^\circ$, 26.595° , 36.49° , and 39.402° . The high and sharp peaks of lanthanum hydroxide indicate that it had a good crystallinity and was successfully loaded on thermally activated coal gangue.

Based on the SEM and TEM of LMGC, the crystal rods of lanthanum hydroxide were uniformly deposited on the surface of thermally activated coal gangue, as shown in Figs. 1c and d. The crystal system was hexagonal. The crystal rods grew in different directions and formed more porous materials.

3.2. Effect of pH value

There are four forms of phosphate (H_3PO_4 , H_2PO_4^- , HPO_4^{2-} , and PO_4^{3-}) in the entire pH range due to its three pKa values of 2.15, 7.20, and 12.33 [33]. The effect of pH value on the phosphate removal by LMGC is shown in Fig. 2. When pH value was 2, the adsorption capacity and removal efficiency of phosphate were only 15.94 mg/g and 31.88%, respectively, because phosphate mainly existed as H_3PO_4 at this pH, where it is difficult to coordinate with lanthanum and adsorb. When the pH increased, the adsorption capacity and removal efficiency of phosphate significantly increased, and they were maximal (i.e., 42.20 mg/g and 84.40%) at pH 5. Phosphate was mainly presented as H_2PO_4^- in the range of pH 3–5; it could be combined with $\text{La}-\text{OH}_2^+$, which is the main form of $\text{La}-\text{OH}$ at low pH, through electrostatic attraction [34], as described in Eqs. (3) and (4):



When pH was higher than 5, the adsorption capacity and removal efficiency of phosphate decreased with the increase in pH. Since the point of zero charge of LMGC is

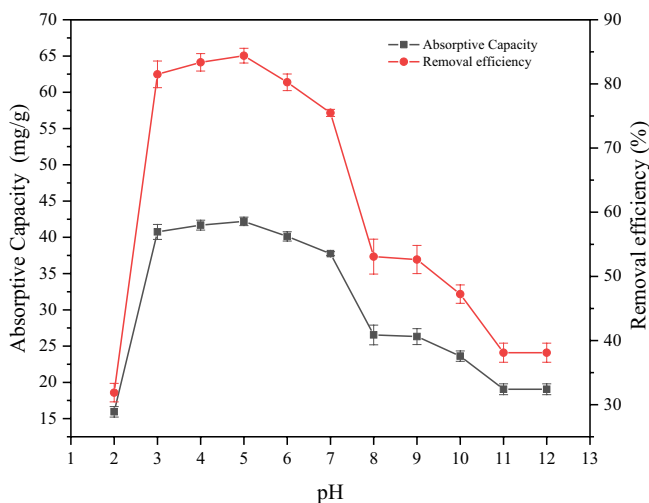


Fig. 2. Effect of pH on adsorption of phosphate ($T = 30^\circ\text{C}$, $\text{pH} = 2\text{--}12$, $C_0 = 50 \text{ mg/L}$, LMGC dosage = 1 g/L, and contact time 2 h).

6.09 (Fig. S1), the surface of the adsorbent was negatively charged when the pH of the solution was higher than 6.09, which resulted in the difficult migration of phosphate to the surface of the adsorbent. Meanwhile, OH^- was highly concentrated on the surface of La at high pH, which might affect the protonation of lanthanum hydroxide, subsequently decrease the removal of phosphate, and compete with phosphonate [35]. In addition, the OH^- concentration increased with the increase in pH, which caused a competitive adsorption with phosphate on the surface of LMGC. Therefore, when $\text{pH} > 7$, the adsorption capacity and removal efficiency of phosphorus rapidly decreased with the increase in pH, and they decreased to 19.05 mg/g and 38.10% at pH 12, respectively. When the pH value was higher than 6.09, the surface of the adsorbent was negatively charged and had electrostatic repulsion with the adsorbate, but adsorption could occur due to the enhancement of complexation, that is, the Lewis acid group interaction played an important role in phosphate removal [36]. The Lewis acid property of La was favorable for its high affinity with oxygen anion in phosphate [37]. Therefore, the Lewis acid group interaction might occur between anion oxygen in phosphate ions and cationic La^{3+} on the surface of the adsorbent to form $\text{La}-\text{O}$. Complexation played an important role in the adsorption of P at high pH value. At this time, the complex formed by lanthanum and phosphate is an inner complex. The adsorption capacity started to decline when pH was 6 in this experiment. The reason may be that the pH value was very close to the zero charge point, the electrostatic attraction effect was not obvious, and the adsorption capacity of the modified material was weakened. The pH value of daily treated water and wastewater was mostly neutral. Therefore, the pH value of subsequent adsorption tests was 7.0.

3.3. Effect of coexisting ions

There are many types of anions and cations in natural water and wastewater, such as Cl^- , F^- , CO_3^{2-} , SO_4^{2-} , NO_3^- , Na^+ , Ca^{2+} , and Mg^{2+} . Their existence might have different effects on the removal of phosphate by LMGC, and the result is shown in Fig. 3.

Cl^- , SO_4^{2-} , NO_3^- , and Na^+ had no significant effect on the removal of phosphate. CO_3^{2-} slightly inhibited the removal of phosphate, possibly since HCO_3^- was the main existing form at pH 7 and could compete with phosphate to adsorb on La. An obvious inhibition was observed in the presence of F^- , and the adsorption capacity of phosphate was only 29.03 mg/g, while the solubility products of $\text{La}(\text{HCO}_3)_3$ and LaPO_4 were approximately 3.7×10^{-23} [38]. Therefore, HCO_3^- and PO_4^{3-} can form competitive adsorption on La to inhibit the adsorption of phosphorus, while the exchange of OH^- further inhibits the adsorption of phosphorus. The solubility product of $\text{La}_2(\text{CO}_3)_3$ [39] was 3.98×10^{-34} , and the inhibition of CO_3^{2-} increased at high pH. F^- had a similar inhibition mechanism to HCO_3^- , and it might form an inner complex with lanthanum hydroxide. In addition, the OH^- that was replaced by F^- might inhibit the adsorption of phosphate on the adsorbent [40]. This result suggests that LMGC had excellent adsorption on phosphate and a multifunctional removal for fluoride.

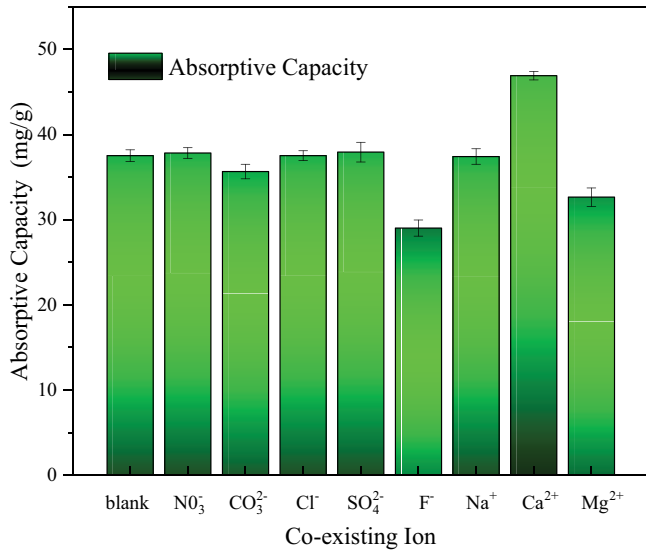


Fig. 3. Effect of coexisting ions on adsorption of phosphate ($T = 30^{\circ}\text{C}$, $\text{pH} = 7.0$, $C_0 = 50 \text{ mg/L}$, LMCG dosage = 1 g/L , and contact time 2 h).

Ca^{2+} had a significant promotion effect on the adsorption of phosphate by LMGC. Possible explanations for this phenomenon include: (1) Ca^{2+} easily formed a complex with PO_4^{3-} [41]; (2) Ca^{2+} was more easily adsorbed on the phosphate-adsorbed LMGC to form a ternary complex of La-P-Ca [42]. It increased the positive charge of the surface and reduced the electrostatic repulsion between LMGC and phosphate after Ca^{2+} was adsorbed on the surface of LMGC; (3) the ternary complex formed by Ca^{2+} and LMGC increases the active site of adsorption of phosphate [43]. The inhibition of Mg^{2+} on the removal of phosphate by LMGC was mainly due to the reactions of Mg^{2+} with La-OH and La-O, which reduced the active site of LMGC [44]. Obviously, the presence of Mg^{2+} could have the same promotion mechanism as Ca^{2+} , but it showed an inhibition effect because this effect was greater than its promotion effect.

3.4. Adsorption kinetics

The removal process of phosphate by LMCG had three stages: rapid adsorption, slow adsorption, and adsorption equilibrium, as shown in Fig. 4a. A higher initial

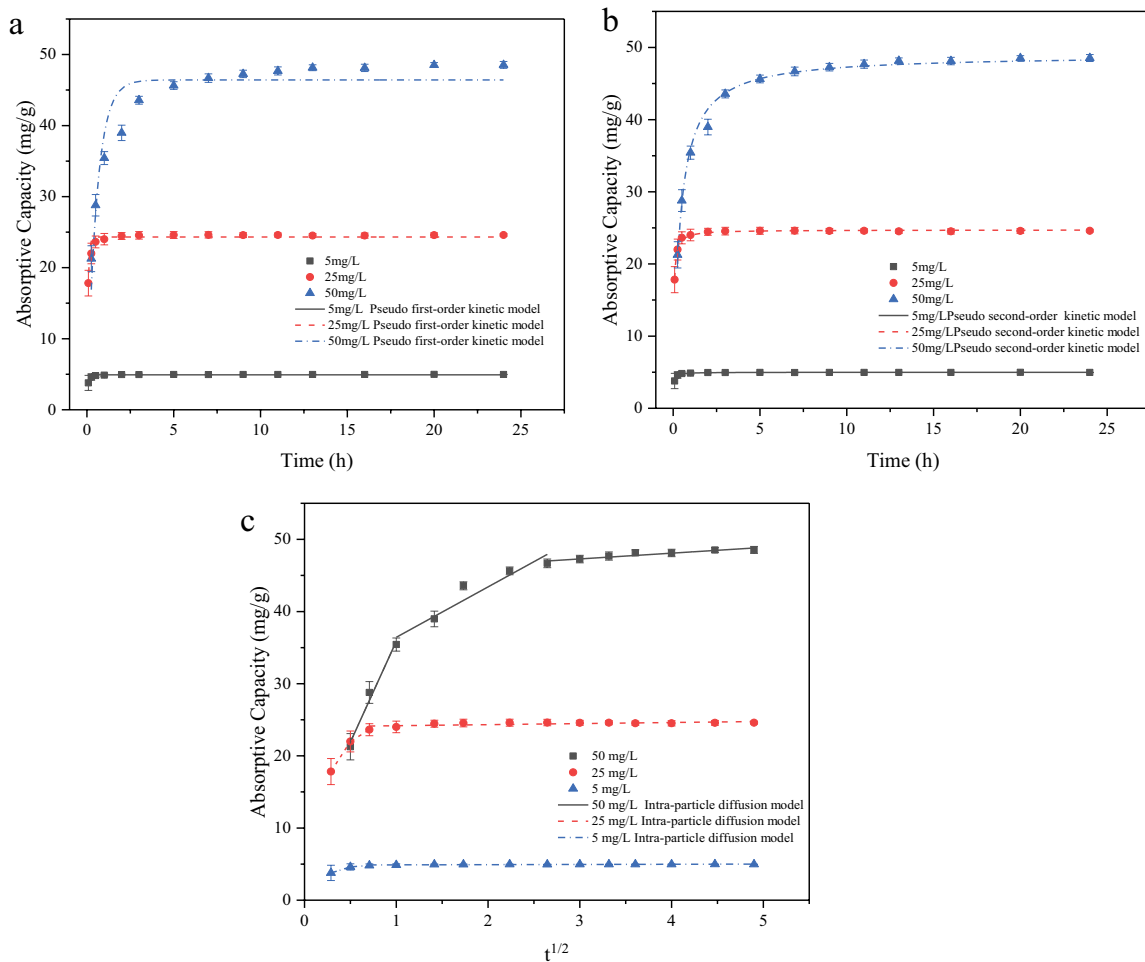


Fig. 4. Kinetic simulation by pseudo-first-order (a), pseudo-second-order (b), and intra-particle diffusion models (c) for phosphate adsorption on LMGC adsorption ($T = 30^{\circ}\text{C}$, $\text{pH} = 7.0$, $C_0 = 5, 25, \text{ and } 50 \text{ mg/L}$, LMCG dosage = 1 g/L , and contact time 0–24 h).

concentration corresponds to a clearer the boundary of the three stages and a larger adsorption capacity of equilibrium.

First, the pseudo-first- and pseudo-second-order kinetics were used to fit the experimental data in Fig. 4a to investigate the adsorption mechanism. The mathematical expressions of the pseudo-first- and pseudo-second-order kinetics are shown in Eqs. (5)–(7).

$$q_t = q_e (1 - e^{-k_1 t}) \quad (5)$$

$$q_t = \frac{k_2 q_e^2 t}{(1 + k_2 q_e t)} \quad (6)$$

$$t_{1/2} = \frac{1}{k_2 Q_e} \quad (7)$$

where q_t and q_e are the adsorption capacities at time t and equilibrium state (mg/g), respectively; k_1 and k_2 are the pseudo-first-order and pseudo-second-order adsorption rate constants, respectively; $t_{1/2}$ is the half adsorption time (h), that is, the time required for the unit adsorption capacity to reach half of the equilibrium adsorption capacity.

The fitting results of the pseudo-first-order kinetic are shown in Fig. 4a and Table 2. The correlation coefficients of the pseudo-first-order kinetic fitting were 0.886, 0.892, and 0.929 at the initial concentrations of 5, 25, and 50 mg/L, respectively. Pseudo-first-order model had the lower R^2 values and the calculated q_e (4.926, 24.322, and 46.420 mg/g) were quite different from the experiment data of 4.971, 24.598, and 48.542 mg/g. Therefore, the pseudo-first-order kinetic model was unfavorable to well-fit the adsorption process, which indicates that the adsorption process was not controlled by a single factor.

Some scholars believe that chemisorption occurs when a pseudo-second-order kinetic model well fits [45]. The fitting results of the pseudo-second-order kinetic model are shown in Fig. 4b and Table 2. The correlation coefficients of the pseudo-second-order kinetic model fitting were 0.988, 0.994, and 0.989 at the initial phosphate concentrations of 5, 25, and 50 mg/L, respectively. Pseudo-second-order model had the higher R^2 values in the two kinetics models and the calculated q_e (4.994, 24.717, and 48.979 mg/g) were close to the experiment data of 4.971, 24.598, and 48.542 mg/g. Thus, the pseudo-second-order kinetic model can be used to well describe the adsorption of LMCG, which indicates that the adsorption of LMCG was a chemisorption process. The half adsorption time $t_{1/2}$ increased from 0.0254 to 0.365 h as the initial phosphate concentration increased from 5 to 50 mg/L, as shown in Table 1, which indicates that the adsorption process was fast.

Generally, the process of adsorption on the solid adsorbent is divided into three stages: diffusion of the liquid film, intraparticle diffusion and adsorption reaction at the active point. The intraparticle diffusion model describes the diffusion process of the adsorbents, and it is expressed by Eq. (8).

$$q_t = k_p t^{1/2} + C \quad (8)$$

where q_t is the adsorption amount at time (mg/g), k_p is the rate constant of intraparticle diffusion (L/h), t is the reaction time (h), and C is the constant of reaction. Some scholars believed that C was directly proportional to the boundary layer film of the adsorbent. A larger C indicates a greater effect of the boundary layer film on adsorption [46]. For a larger k_p , it is easier for the adsorbate to diffuse inside the adsorbent. k_p can be obtained from the slope of the line of

Table 2
Fitting results of the dynamic model of LMCG

Dynamic model	Parameters	5 mg/L	25 mg/L	50 mg/L
Pseudo-first-order kinetic model	q_e (mg/L)	4.926	24.322	46.420
	k_1 (h ⁻¹)	17.024	15.068	1.811
	R^2	0.929	0.892	0.886
Pseudo-second-order kinetic model	q_e (mg/L)	4.994	24.717	48.979
	k_2 (h ⁻¹)	7.899	1.291	0.056
	$t_{1/2}$ (h)	0.0254	0.0313	0.365
	R^2	0.988	0.994	0.989
Intra-particle diffusion model				
Step 1	k_p	3.93	19.737	27.94
	C	2.643	12.131	7.937
	R^2	1	1	0.982
Step 2	k_p	0.975	7.846	6.985
	C	4.121	18.076	29.445
	R^2	1	1	0.921
Step 3	k_p	0.027	0.148	0.799
	C	4.87	24.031	44.891
	R^2	0.532	0.44	0.88

$q_t - t^{1/2}$. According to the intraparticle diffusion equation, q_t has a linear relationship with $t^{1/2}$. If the straight line passes through the origin, the rate of adsorption is controlled only by intraparticle diffusion. If there are several straight lines whose intercept is not necessarily 0, adsorption is involved in many processes, including liquid film diffusion, internal particle diffusion, and adsorption equilibrium [47].

The fitting results of the intraparticle diffusion model are shown in Fig. 4c and Table 2. The adsorption process of phosphorus by LMGC was clearly divided into three stages. The first stage was a fast adsorption process, and the adsorption amount rapidly increased with the increase in adsorption time. In this stage, liquid film diffusion might occurred. In the second stage, particle diffusion played a major role and the adsorption speed decreased. The third stage was an equilibrium process. With the increase in adsorption time, the adsorption capacity could no longer increase. The linear intercept of each stage fitted by the internal particle diffusion kinetic model was not zero, which suggests that the adsorption rate was controlled by both liquid film diffusion and internal particle diffusion.

3.5. Adsorption isotherm

Langmuir isotherm adsorption model [48] assumes that all adsorption sites are equivalent. Each site can only adsorb one molecule of adsorbate. The surface of the adsorbent is uniform. In the process, only single-layer adsorption occurs. The specific expression is shown in Eq. (9). Separation coefficient R_L is developed from Langmuir isothermal adsorption model and expressed by Eq. (10):

$$q_e = \frac{q_m K_L C_e}{1 + K_L C_e} \tag{9}$$

$$R_L = \frac{1}{1 + K_L C_0} \tag{10}$$

where q_e and q_m are the equilibrium and saturated adsorption capacities (mg/g), respectively; K_L is the binding constant, C_0 and C_e are the initial and equilibrium concentrations of the adsorbate (mg/L), respectively; R_L is the separation coefficient, which is related to the efficiency of adsorption and difficulty of adsorption. If $0 < R_L < 1$, the adsorption process is easy. If $R_L > 1$, the adsorption process is difficult [48–50].

The fitting results of Langmuir isothermal adsorption model are shown in Fig. 5a and Table 3. The correlation coefficient of Langmuir isotherm was relatively high, which indicates that the adsorption was a single-molecular-layer adsorption, and the surface of the adsorbent was relatively uniform. The maximum single-layer adsorption capacity of LMGC for phosphate at 20°C, 30°C, and 40°C was 78.66, 80.58, and 83.83 mg/g, respectively, which was close to the experimental results. The separation coefficient (R_L) of LMGC for phosphate at different temperatures was calculated using Eq. (13), and it was far less than 1 at 20°C, 30°C, and 40°C. R_L is less than 1 and decreases with the increase in PO_4^{3-} initial concentration, which indicates that the adsorption process was easy, and it was difficult to separate the adsorbent and adsorbate because there was chemisorption in the adsorption process, and the chemisorption energy was higher than physical adsorption.

Freundlich isotherm model is an empirical formula based on the process of solid adsorbing gas [51], which is based on the adsorption process of gas on solid. It is more suitable to describe the adsorption behavior of a low-concentration adsorbate on a heterogeneous adsorbent surface [52]. The expression of Freundlich isotherm is shown in Eq. (11).

$$q_e = K_f C_e^{1/n_f} \tag{11}$$

where q_e is the equilibrium and saturated adsorption capacity (mg/g), K_f is the constant related to the adsorption capacity and adsorption strength, C_e is the initial and equilibrium concentration of the adsorbate (mg/L) and is

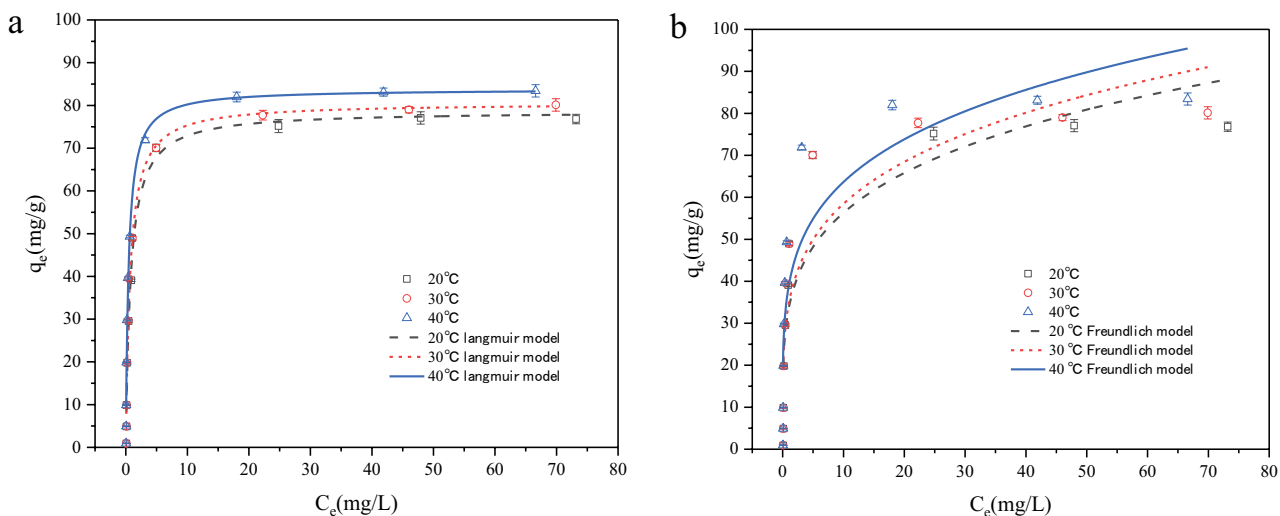


Fig. 5. Langmuir isotherm model (a) and Freundlich isotherms model (b) isothermal fittings for phosphate adsorption on LMGC ($T = 20^\circ\text{C}, 30^\circ\text{C},$ and 40°C , $\text{pH} = 7.0$, $C_0 = 1\text{--}150$ mg/L, LMGC dosage = 1 g/L, and contact time 24 h).

Table 3
Parameters of the LMGC adsorption isotherm

Isotherm model	Parameters	20°C	30°C	40°C
Langmuir model	q_{\max} (mg/L)	78.66	80.58	83.83
	K_L (L/mg)	1.27	1.432	2.223
	R^2	0.987	0.985	0.986
	K_F	33.561	34.624	38.908
Freundlich model	$1/n_F$	0.225	0.228	0.214
	R^2	0.819	0.823	0.829

Freundlich constant. Larger values of K_F and n_F indicate that the adsorbent has better adsorption performance. It is difficult to adsorb if n_F is less than 1. The adsorption is moderately difficult if n_F is 1–2. If n_F is between 2 and 10, it is easy to adsorb [53].

The fitting results of Freundlich isothermal adsorption model are shown in Fig. 5b and Table 3. The correlation coefficient of Freundlich isotherm was lower than that of Langmuir isotherm. The value of K_F was 20°C < 30°C < 40°C, which indicates that the adsorption capacity of LMCG was greater at higher temperature. The n_F values of the model were 4.44, 4.39, and 4.67, which suggests the adsorption of phosphate by LMCG was favorable. However, Freundlich model has a lower correlation coefficient than Langmuir model, so Freundlich model may not accurately reflect the process of phosphate adsorption by LMCG. Langmuir model can better describe the isotherm adsorption of phosphate.

3.6. Adsorption thermodynamics

The spontaneity of the adsorption reaction, disorder degree of the reaction system, and characteristics of the thermal change in the adsorption process were determined by enthalpy change (ΔH°), entropy change (ΔS°), and Gibbs free energy (ΔG°), respectively, as shown in Eqs. (12)–(15) [54,55].

$$\Delta G^\circ = -RT \ln K_c \quad (12)$$

$$\ln K_c = -\frac{\Delta H^\circ}{RT} + \frac{\Delta S^\circ}{R} \quad (13)$$

$$\Delta G^\circ = \Delta H^\circ - T\Delta S^\circ \quad (14)$$

$$K_c = \left(\frac{q_e}{C_e}\right) \left(\frac{W}{V}\right) \quad (15)$$

where q_e is the adsorption amount at equilibrium (mg/g); C_e is the concentration of the adsorbate in the solution at equilibrium (mg/L); R is the gas constant (0.0083145 kJ/(mol K)); T is the adsorption reaction temperature (K); K_c is the equilibrium constant, which can be calculated from Eq. (15); W is the added mass of LMGC (g); V is the volume of the adsorbate solution (L). ΔG° can be calculated from Eq. (12). ΔH° and ΔS° can be obtained by linear fitting of $\ln K_c$ to $1/T$ from Eq. (13).

The calculation results are shown in Table 4. ΔG° of the adsorption reaction at 20°C, 30°C, and 40°C was negative

Table 4
Thermodynamic parameters of the adsorption process at the initial concentration of 20 mg/L

T (K)	ΔG° (kJ/mol)	ΔH° (kJ/mol)	ΔS° (kJ/mol)
293.15	-11.8752	23.581	0.115181
303.15	-11.63		
313.15	-13.4994		

when the initial concentration of phosphate was 20 mg/L, which indicates that this adsorption process was spontaneous. Both ΔH° and ΔS° were positive, which suggests that this adsorption was an endothermic reaction, which is consistent with the conclusion that the adsorption capacity enhanced with the increase in temperature. All calculated ΔG° values were negative at different initial concentrations of phosphate, which further suggests that the adsorption process by LMCG was spontaneous. The decrease in ΔG° with the increase in temperature indicates that the adsorption process was endothermic [56].

3.7. Study on the adsorption mechanism

The ATR-FTIR spectra of LMCG before and after phosphate adsorption are shown in Fig. 1a. The absorption peak at 3,607 cm^{-1} , which belonged to the stretching vibration of the hydroxyl group in $\text{La}(\text{OH})_3$, disappeared after adsorption, which indicates that $\text{La}(\text{OH})_3$ participated in the reaction during the adsorption process, and OH^- was replaced and entered the liquid phase [43]. There were two new peaks at 1,005 and 1,052 cm^{-1} [57–59], which belonged to the stretching vibration of P–O of $\text{H}_2\text{PO}_4^{1-}$ and HPO_4^{2-} , respectively. Although the absorption peaks at 853, 634, and 558 cm^{-1} of La–O disappeared after adsorption, several sharp absorption peaks near 857, 610, and 537 cm^{-1} appeared, and they might belong to the bending vibration of O–P–O in the complex of PO_4^{3-} and La^{3+} [31]. The peaks at 610 and 537 cm^{-1} might be the vibration of lanthanum phosphate formed by the exchange of $-\text{OH}$ with PO_4^{3-} in La–OH [59]. The peak at 857 cm^{-1} might be the bending vibration of O–P–O produced by the coordination of PO_4^{3-} with O–La [31]. These results indicate that the adsorption of phosphate by LMCG was mainly caused by ion exchange and coordination to form insoluble LaPO_4 , $\text{La}_2(\text{HPO}_4)_3$, and $\text{La}(\text{H}_2\text{PO}_4)_3$.

The XRD analysis of LMCG before and after adsorption also proves that a chemical adsorption reaction occurred, as shown in Fig. 2b. The disappearance of the peak at 15.719°, reduction of the characteristic peak of lanthanum hydroxide at 27.880°, and the appearance of several new characteristic peaks of lanthanum phosphate at 119.82°, 25.301°, 31.2°, and 53.96° indicate that lanthanum hydroxide participated in the chemical adsorption reaction to generate LaPO_4 .

Compared with the full XPS spectrum of LMCG before adsorption, a characteristic peak obviously appeared at 132.8 eV after adsorption, as presented in Fig. 6, which indicates that phosphate was adsorbed on the surface of LMCG. The peak of C1s at 284.6 eV increased after adsorption, which might be caused by the adsorption of C from aqueous solution or air during the adsorption process or drying process. This result is consistent with the FTIR analysis results.

The fine spectra of O1s and La3d before and after the phosphate adsorption were analyzed and are shown in Fig. S2. The O1s peak at 531.2 eV shifted to 531.4 eV and significantly increased (Fig. S2a), which indicates that phosphate was adsorbed on the material. The peak of La3d_{5/2} shifted from 835.4 to 835.6 eV and decreased (Fig. S2b), which might be due to the transfer of valence band of coordination atom to the 4-orbital of La [60]. These results suggest that there was a strong force between lanthanum and phosphate, and the La–O–P bond was formed [59,61,62].

The O1s fine spectra before and after the adsorption of phosphate by LMCG were fitted using the XPSpeak4.1 software, and the results are shown in Figs. 7a and b. According to the binding energy of different types of oxygen, O1s can be divided into lattice oxygen (M–O), hydroxyl oxygen (M–OH), and combined water oxygen (H₂O).

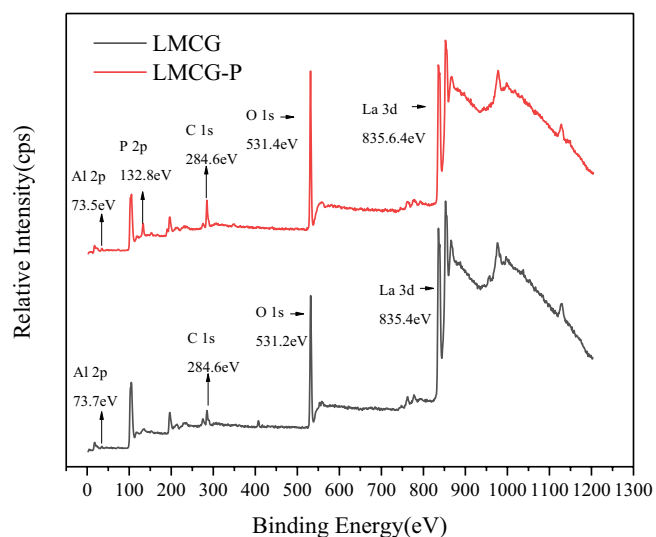


Fig. 6. Survey scan XPS spectra for LMCG before and after phosphate adsorption (LMCG before phosphate adsorption and LMCG-P after phosphate adsorption).

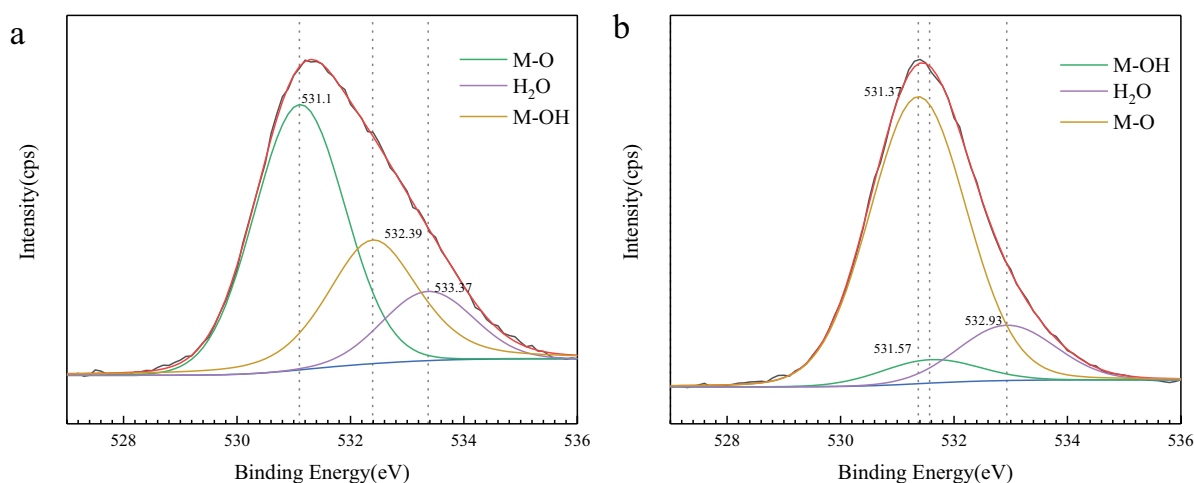


Fig. 7. Wide scan XPS spectra of O1s of LMCG before and after phosphate adsorption (a) XPS spectra of O1s before phosphate adsorption and (b) XPS spectra of O1s after phosphate adsorption.

Fig. 7 shows that the peak positions of various oxygen forms significantly changed before and after adsorption, which indicates that there was a certain reaction between phosphate and oxygen in the adsorbent. The relative content of M–O increased from 55.32% to 79.10% after adsorption, which indicates that a large amount of phosphate was adsorbed on the surface of the adsorbent. The decrease in relative content of M–OH from 30.39% to 6.22% indicates that the hydroxyl groups of LMCG participated in the reaction and were replaced, which is consistent with the ATR-FTIR results. These results also suggest that the presence of hydroxyl groups on the surface of LMCG had a positive effect on the removal of phosphate. In this study, the stoichiometric ratio of hydroxyl groups on the surface of LMCG before and after the adsorption of phosphate was 4.89, which suggests that the complex formed through the adsorption reaction was a bidentate inner layer complex [63].

Based on the results of adsorption kinetics, adsorption isotherm and adsorption thermodynamics and characterization of LMCG before and after the adsorption by ATR-FTIR, XRD, and XPS, the removal mechanism of phosphate by LMCG was tentatively proposed, as shown in Fig. 9. First, the main active site in LMCG was the loaded lanthanum hydroxide on the surface. Second, the removal of phosphate by LMCG mainly depended on chemical adsorption. At the initial pH value of 7.0, phosphate mainly existed in the forms of H₂PO₄⁻, HPO₄²⁻, and a small amount of PO₄³⁻, which could experience ligand exchange reactions with lanthanum hydroxide. In addition, they might experience a coordination reaction with La in the La–O bond in the structural layer of LMCG according to the ATR-FTIR analysis. Finally, a bidentate inner complex was formed after the phosphate adsorption by LMCG. The schematic diagram of the dephosphorization mechanism is shown in Fig. 8.

4. Conclusions

LMCG was successfully prepared and applied to remove phosphate from water. Langmuir model and the pseudo-second-order model were well fitted in the adsorption

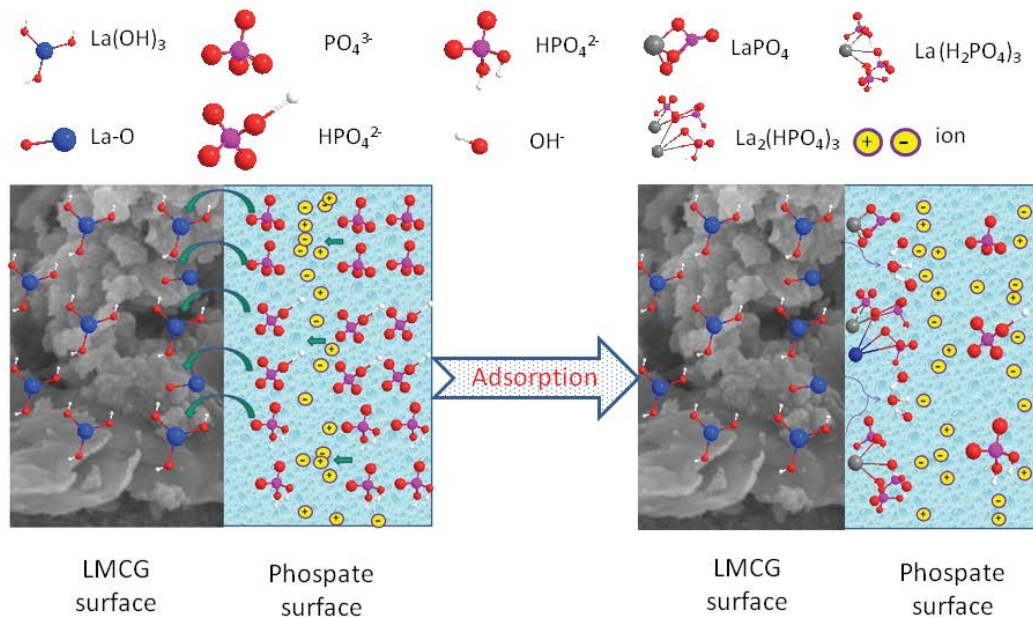


Fig. 8. Schematic mechanism of phosphate adsorption on LMCG.

process. The maximum phosphate adsorption capacity fitted by Langmuir model was 78.66, 80.58, and 83.83 mg/g at 20°C, 30°C, and 40°C, respectively. The thermodynamic study showed that the adsorption process was a spontaneous endothermic reaction. The fitting results of the pseudo-second-order dynamics model show that the adsorption type was chemical adsorption. The intraparticle diffusion model indicates that the adsorption process of phosphate by LMCG was divided into three steps. The study on the effect of coexisting ions demonstrates that LMCG was highly selective to phosphate. Combined with the adsorption experiments and characterization results by XPS, XRD, and ATR-FITR, the main adsorption mechanism was proposed, that is, the formation of inner complexes through ligand exchange. LMCG is an excellent phosphate-removing agent with low cost, high adsorption capacity, high selectivity, and environmental friendliness, which can be widely used in a natural water body, municipal sewage, and industrial wastewater.

Author contributions

Conceptualization: Jianmin Zhou, Yongsheng Fu, and Yiqing Liu; Data curation: Jianmin Zhou, Mengyao Zhang, and Shuhang Ding; Formal analysis: Jianmin Zhou and Yiqing Liu; Investigation: Jianmin Zhou and Mengyao Zhang; Methodology: Jianmin Zhou, Yongsheng Fu, and Yiqing Liu; Project administration: Jianmin Zhou; Resources, Jianmin Zhou and Yongsheng Fu; Software: Shuhang Ding and Li Zhao; Validation: Yongsheng Fu; Visualization: Mengyao Zhang, and Shuhang Ding; Writing the original draft: Jianmin Zhou; Writing, review, and editing: Yiqing Liu and Li Zhao.

Acknowledgment

The authors thank the editor and reviewers for their very useful suggestions and comments.

References

- [1] Z. Wang, Z. Zhang, J. Zhang, Y. Zhang, H. Liu, S. Yan, Large-scale utilization of water hyacinth for nutrient removal in Lake Dianchi in China: the effects on the water quality, macrozoobenthos and zooplankton, *Chemosphere*, 89 (2012) 1255–1261.
- [2] W.H. Schlesinger, *Biogeochemistry: An Analysis of Global Change*, Academic Press, California, USA, 1997.
- [3] P. Dillon, F. Rigler, A simple method for predicting the capacity of a lake for development based on lake trophic status, *J. Fish. Res. Board Can.*, 32 (1975) 1519–1531.
- [4] P. Lin, L. Guo, Dynamic changes in the abundance and chemical speciation of dissolved and particulate phosphorus across the river-lake interface in southwest Lake Michigan, *Limnol. Oceanogr.*, 61 (2016) 771–789.
- [5] E. Osuch, A. Osuch, S. Podsiadłowski, L. Piechnik, D. Chwirot, Project of coagulant dispenser in pulverization aerator with wind drive, *J. Ecol. Eng.*, 18 (2017) 192–198.
- [6] F. Araújo, H. Rodrigues dos Santos, V. Becker, J.L. Attayde, The use of polyaluminium chloride as a restoration measure to improve water quality in tropical shallow lakes, *Acta Limnol. Bras.*, 30 (2018) e109, doi: 10.1590/s2179-975x8416.
- [7] H. Yin, M. Han, W. Tang, Phosphorus sorption and supply from eutrophic lake sediment amended with thermally-treated calcium-rich attapulgite and a safety evaluation, *Chem. Eng. J.*, 285 (2016) 671–678.
- [8] C. Li, H. Yu, S. Tabassum, L. Li, D. Wu, Z. Zhang, H. Kong, P. Xu, Effect of calcium silicate hydrates (CSH) on phosphorus immobilization and speciation in shallow lake sediment, *Chem. Eng. J.*, 317 (2017) 844–853.
- [9] T. Bao, T.-h. Chen, C. Qing, J. Jin Xie, R.L. Frost, Development and application of *Palygorskite porous* ceramsite in a biological aerated filter (BAF), *Desal. Water Treat.*, 57 (2016) 1790–1803.
- [10] Q. Zhang, F. Sun, W. Dong, Nitrobenzene removal from micro-polluted water resource by a submerged MBR and the importance of activated sludge, *Desal. Water Treat.*, 57 (2016) 11300–11308.
- [11] Y. Zhang, M.S. Islam, K.N. McPhedran, S. Dong, E.M. Rashed, M.M. El-Shafei, A.M. Noureldin, M.G. El-Din, A comparative study of microbial dynamics and phosphorus removal for a two side-stream wastewater treatment processes, *RSC Adv.*, 7 (2017) 45938–45948.

- [12] J. Petrovic, S. Acic, D. Obratov-Petkovic, Z.D. Stevanovic, R. Ristic, N. Stavretovic, Ecological features of vascular flora on ski trails on NP Kopaonik mountain, Serbia, *Fresenius Environ. Bull.*, 25 (2016) 2985–2990.
- [13] N. Yeh, P. Yeh, Y.-H. Chang, Artificial floating islands for environmental improvement, *Renewable Sustainable Energy Rev.*, 47 (2015) 616–622.
- [14] B. Lu, Z. Xu, J. Li, X. Chai, Removal of water nutrients by different aquatic plant species: an alternative way to remediate polluted rural rivers, *Ecol. Eng.*, 110 (2018) 18–26.
- [15] D. Gu, H. Xu, Y. He, F. Zhao, M. Huang, Remediation of urban river water by *Pontederia cordata* combined with artificial aeration: organic matter and nutrients removal and root-adhered bacterial communities, *Int. J. Phytoremed.*, 17 (2015) 1105–1114.
- [16] T. Fang, S. Bao, X. Sima, H. Jiang, W. Zhu, W. Tang, Study on the application of integrated eco-engineering in purifying eutrophic river waters, *Ecol. Eng.*, 94 (2016) 320–328.
- [17] H. Xiao, N. Liu, K. Tian, S. Liu, F. Ge, Accelerated effects of nano-ZnO on phosphorus removal by *Chlorella vulgaris*: formation of zinc phosphate crystallites, *Sci. Total Environ.*, 635 (2018) 559–566.
- [18] K. Kim, D. Kim, T. Kim, B.-G. Kim, D. Ko, J. Lee, Y. Han, J.C. Jung, H.B. Na, Synthesis of mesoporous lanthanum hydroxide with enhanced adsorption performance for phosphate removal, *RSC Adv.*, 9 (2019) 15257–15264.
- [19] Q. Xie, Y. Li, Z. Lv, H. Zhou, X. Yang, J. Chen, H. Guo, Effective adsorption and removal of phosphate from aqueous solutions and eutrophic water by Fe-based MOFs of MIL-101, *Sci. Rep.*, 7 (2017), doi: 10.1038/s41598-017-03526-x.
- [20] Q. Cui, G. Jiao, J. Zheng, T. Wang, G. Wu, G. Li, Synthesis of a novel magnetic *Caragana korshinskii* biochar/Mg-Al layered double hydroxide composite and its strong adsorption of phosphate in aqueous solutions, *RSC Adv.*, 9 (2019) 18641–18651.
- [21] Z. Zhong, G. Yu, W. Mo, C. Zhang, H. Huang, S. Li, M. Gao, X. Lu, B. Zhang, H. Zhu, Enhanced phosphate sequestration by Fe(III) modified biochar derived from coconut shell, *RSC Adv.*, 9 (2019) 10425–10436.
- [22] M. Pan, X. Lin, J. Xie, X. Huang, Kinetic, equilibrium and thermodynamic studies for phosphate adsorption on aluminum hydroxide modified palygorskite nano-composites, *RSC Adv.*, 7 (2017) 4492–4500.
- [23] Z. Zha, Y. Ren, S. Wang, Z. Qian, L. Yang, P. Cheng, Y. Han, M. Wang, Phosphate adsorption onto thermally dehydrated aluminate cement granules, *RSC Adv.*, 8 (2018) 19326–19334.
- [24] M. Kasprzyk, M. Gajewska, Phosphorus removal by application of natural and semi-natural materials for possible recovery according to assumptions of circular economy and closed circuit of P, *Sci. Total Environ.*, 650 (2019) 249–256.
- [25] D. Guaya, C. Valderrama, A. Farran, C. Armijos, J.L. Cortina, Simultaneous phosphate and ammonium removal from aqueous solution by a hydrated aluminum oxide modified natural zeolite, *Chem. Eng. J.*, 271 (2015) 204–213.
- [26] S. Vasudevan, J. Lakshmi, The adsorption of phosphate by graphene from aqueous solution, *Rsc Adv.*, 2 (2012) 5234–5242.
- [27] J.W. Lim, K.F. Lee, T.S.Y. Chong, L.C. Abdullah, M.A. Razak, C. Tezara, Phosphorus removal by electric arc furnace steel slag adsorption, *IOP Conf. Ser.: Mater. Sci. Eng.*, 257 (2017) 012063, doi: 10.1088/1757-899X/257/1/012063.
- [28] L. Yang, Study on comprehensive utilization of coal gangue, *China Petrochem.*, 11 (2017) 54–55.
- [29] J. Li, The Influence of Coal Gangue Accumulation on Surrounding Soil in Yangquan Mining Area, Shanxi Province, *Huabei Land and Resources*, 2014, pp. 96–98.
- [30] L. González-Rovira, J. Sanchez-Amaya, M. Lopez-Haro, A. Hungria, Z. Boukha, S. Bernal, F. Botana, Formation and characterization of nanotubes of La(OH)₃ obtained using porous alumina membranes, *Nanotechnology*, 19 (2008) 495305, doi: 10.1088/0957-4484/19/49/495305.
- [31] P.R. Kumar, T.M. Maharajan, M. Chinnsamy, A.P. Prabu, J.A. Suthagar, K.S. Kumar, Hydroxyl radical scavenging activity of La₂O₃ nanoparticles, *Pharma Innovation J.*, 8 (2019) 759–763.
- [32] M. Aghazadeh, B. Arhami, A.-A.M. Barmi, M. Hosseini-fard, D. Gharailou, F. Fathollahi, La(OH)₃ and La₂O₃ nanospindles prepared by template-free direct electrodeposition followed by heat-treatment, *Mater. Lett.*, 115 (2014) 68–71.
- [33] E. Zong, D. Wei, H. Wan, S. Zheng, Z. Xu, D. Zhu, Adsorptive removal of phosphate ions from aqueous solution using zirconia-functionalized graphite oxide, *Chem. Eng. J.*, 221 (2013) 193–203.
- [34] Y. He, H. Lin, Y. Dong, L. Wang, Preferable adsorption of phosphate using lanthanum-incorporated porous zeolite: characteristics and mechanism, *Appl. Surf. Sci.*, 426 (2017) 995–1004.
- [35] W. Xiong, J. Tong, Z. Yang, G. Zeng, Y. Zhou, D. Wang, P. Song, R. Xu, C. Zhang, M. Cheng, Adsorption of phosphate from aqueous solution using iron-zirconium modified activated carbon nanofiber: performance and mechanism, *J. Colloid Interface Sci.*, 493 (2017) 17–23.
- [36] N.Y. Acelas, B.D. Martin, D. López, B. Jefferson, Selective removal of phosphate from wastewater using hydrated metal oxides dispersed within anionic exchange media, *Chemosphere*, 119 (2015) 1353–1360.
- [37] R.S. Wu, K.H. Lam, J.M. Lee, T. Lau, Removal of phosphate from water by a highly selective La(III)-chelex resin, *Chemosphere*, 69 (2007) 289–294.
- [38] S. Dong, Y. Wang, Y. Zhao, X. Zhou, H. Zheng, La³⁺/La(OH)₃ loaded magnetic cationic hydrogel composites for phosphate removal: effect of lanthanum species and mechanistic study, *Water Res.*, 126 (2017) 433–441.
- [39] X. Zhang, F. Sun, J. He, H. Xu, F. Cui, W. Wang, Robust phosphate capture over inorganic adsorbents derived from lanthanum metal organic frameworks, *Chem. Eng. J.*, 326 (2017) 1086–1094.
- [40] W. Shi, Y. Fu, W. Jiang, Y. Ye, J. Kang, D. Liu, Y. Ren, D. Li, C. Luo, Z. Xu, Enhanced phosphate removal by zeolite loaded with Mg-Al-La ternary (hydr) oxides from aqueous solutions: performance and mechanism, *Chem. Eng. J.*, 357 (2019) 33–44.
- [41] B. Lin, M. Hua, Y. Zhang, W. Zhang, L. Lv, B. Pan, Effects of organic acids of different molecular size on phosphate removal by HZO-201 nanocomposite, *Chemosphere*, 166 (2017) 422–430.
- [42] M.T. Atouei, R. Rahnemaie, E.G. Kalanpa, M.H. Davoodi, Competitive adsorption of magnesium and calcium with phosphate at the goethite water interface: Kinetics, equilibrium and CD-MUSIC modeling, *Chem. Geol.*, 437 (2016) 19–29.
- [43] P. Koilraj, K. Sasaki, Selective removal of phosphate using La-porous carbon composites from aqueous solutions: batch and column studies, *Chem. Eng. J.*, 317 (2017) 1059–1068.
- [44] C.-C. Lin, *Original Equipment Manufacturing Contract and Three-Way Bargaining: Cooperation, Control, and the Opportunism Within*, M. Heidemann, J. Lee, Eds., *The Future of the Commercial Contract in Scholarship and Law Reform*, Springer, Cham, 2018, pp. 167–187.
- [45] Y. Ho, G. McKay, A comparison of chemisorption kinetic models applied to pollutant removal on various sorbents, *Process Saf. Environ. Prot.*, 76 (1998) 332–340.
- [46] G. McKay, M. Otterburn, A. Sweeney, The removal of colour from effluent using various adsorbents-III. Silica: rate processes, *Water Res.*, 14 (1980) 15–20.
- [47] A. Pandiarajan, R. Kamaraj, S. Vasudevan, S. Vasudevan, OPAC (orange peel activated carbon) derived from waste orange peel for the adsorption of chlorophenoxyacetic acid herbicides from water: adsorption isotherm, kinetic modelling and thermodynamic studies, *Bioresour. Technol.*, 261 (2018) 329–341.
- [48] Y. Sharma, V. Srivastava, S. Upadhyay, C. Weng, Alumina nanoparticles for the removal of Ni(II) from aqueous solutions, *Ind. Eng. Chem. Res.*, 47 (2008) 8095–8100.
- [49] Y.M. Magdy, H. Altaher, E. ElQada, Removal of three nitrophenols from aqueous solutions by adsorption onto char ash: equilibrium and kinetic modeling, *Appl. Water Sci.*, 8 (2018) 1–15, doi: 10.1007/s13201-018-0666-1.
- [50] A.C. Martins, O. Pezoti, A.L. Cazetta, K.C. Bedin, D.A. Yamazaki, G.F. Bandoch, T. Asefa, J.V. Visentainer, V.C. Almeida, Removal of tetracycline by NaOH-activated carbon produced from

- macadamia nut shells: kinetic and equilibrium studies, *Chem. Eng. J.*, 260 (2015) 291–299.
- [51] R.J. Umpleby, S.C. Baxter, Y. Chen, R.N. Shah, K.D. Shimizu, Characterization of molecularly imprinted polymers with the Langmuir-Freundlich isotherm, *Anal. Chem.*, 73 (2001) 4584–4591.
- [52] P. Wang, X. Wang, S. Yu, Y. Zou, J. Wang, Z. Chen, N.S. Alharbi, A. Alsaedi, T. Hayat, Y. Chen, Silica coated Fe_3O_4 magnetic nanospheres for high removal of organic pollutants from wastewater, *Chem. Eng. J.*, 306 (2016) 280–288.
- [53] J. Ma, J. Qi, C. Yao, B. Cui, T. Zhang, D. Li, A novel bentonite-based adsorbent for anionic pollutant removal from water, *Chem. Eng. J.*, 200 (2012) 97–103.
- [54] E.C. Lima, A. Hosseini-Bandegharai, J.C. Moreno-Piraján, I. Anastopoulos, A critical review of the estimation of the thermodynamic parameters on adsorption equilibria. Wrong use of equilibrium constant in the Van't Hoof equation for calculation of thermodynamic parameters of adsorption, *J. Mol. Liq.*, 273 (2019) 425–434.
- [55] A. Mandal, S.K. Das, Phenol adsorption from wastewater using clarified sludge from basic oxygen furnace, *J. Environ. Chem. Eng.*, 7 (2019) 103259, doi: 10.1016/j.jece.2019.103259.
- [56] K.P. Singh, A. Malik, S. Sinha, P. Ojha, Liquid-phase adsorption of phenols using activated carbons derived from agricultural waste material, *J. Hazard. Mater.*, 150 (2008) 626–641.
- [57] J. Xie, Z. Wang, S. Lu, D. Wu, Z. Zhang, H. Kong, Removal and recovery of phosphate from water by lanthanum hydroxide materials, *Chem. Eng. J.*, 254 (2014) 163–170.
- [58] L. Kong, Y. Tian, N. Li, Y. Liu, J. Zhang, J. Zhang, W. Zuo, Highly-effective phosphate removal from aqueous solutions by calcined nano-porous palygorskite matrix with embedded lanthanum hydroxide, *Appl. Clay Sci.*, 162 (2018) 507–517.
- [59] X. Liu, E. Zong, W. Hu, P. Song, J. Wang, Q. Liu, Z. Ma, S. Fu, Lignin-derived porous carbon loaded with $\text{La}(\text{OH})_3$ nanorods for highly efficient removal of phosphate, *ACS Sustainable Chem. Eng.*, 7 (2018) 758–768.
- [60] C. Zhang, Y. Li, F. Wang, Z. Yu, J. Wei, Z. Yang, C. Ma, Z. Li, Z. Xu, G. Zeng, Performance of magnetic zirconium-iron oxide nanoparticle in the removal of phosphate from aqueous solution, *Appl. Surf. Sci.*, 396 (2017) 1783–1792.
- [61] L. Kong, Y. Tian, Z. Pang, X. Huang, M. Li, R. Yang, N. Li, J. Zhang, W. Zuo, Synchronous phosphate and fluoride removal from water by 3D rice-like lanthanum-doped La@MgAl nanocomposites, *Chem. Eng. J.*, 371 (2019) 893–902.
- [62] H. Qiu, C. Liang, J. Yu, Q. Zhang, M. Song, F. Chen, Preferable phosphate sequestration by nano- $\text{La}(\text{III})$ (hydr) oxides modified wheat straw with excellent properties in regeneration, *Chem. Eng. J.*, 315 (2017) 345–354.
- [63] S. Wan, S. Wang, Y. Li, B. Gao, Functionalizing biochar with Mg-Al and Mg-Fe layered double hydroxides for removal of phosphate from aqueous solutions, *J. Ind. Eng. Chem.*, 47 (2017) 246–253.

Supplementary information

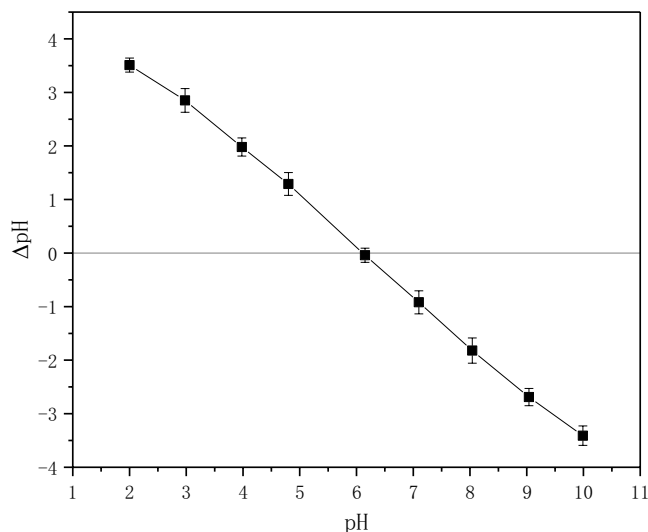


Fig. S1. Plot for determination of zero point charge for the LMCG.

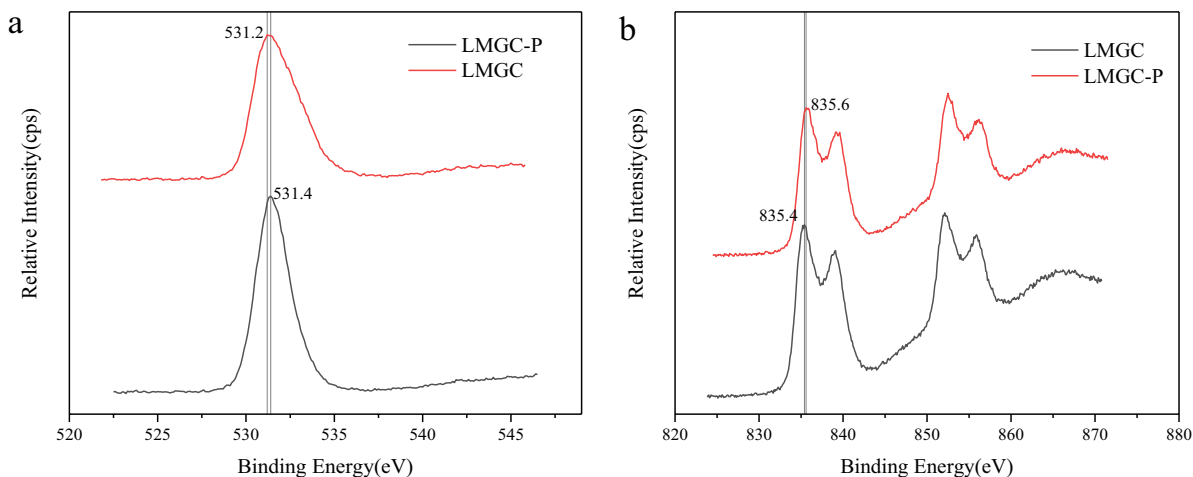


Fig. S2. Wide scan XPS spectra of O1s (a) and La3d (b) of LMCG before and after phosphate adsorption (LMGC wide scan XPS spectra before phosphate adsorption and LMGC-P wide scan XPS spectra after phosphate adsorption).